

Modelling the Zambezi River plume

FPJ Nehama & CJC Reason

To cite this article: FPJ Nehama & CJC Reason (2015) Modelling the Zambezi River plume, African Journal of Marine Science, 37:4, 593-604, DOI: [10.2989/1814232X.2015.1113202](https://doi.org/10.2989/1814232X.2015.1113202)

To link to this article: <http://dx.doi.org/10.2989/1814232X.2015.1113202>



Published online: 20 Dec 2015.



Submit your article to this journal [↗](#)



View related articles [↗](#)



View Crossmark data [↗](#)

Modelling the Zambezi River plume

FPJ Nehama and CJC Reason*

Department of Oceanography, University of Cape Town, Cape Town, South Africa

* Corresponding author, e-mail: chris.reason@uct.ac.za

A model for the Zambezi River plume, the largest on the Indian Ocean coast of Africa, is presented and the results of experiments with different discharges and wind forcings are analysed. Although the river plays an important role in the southern African economy through power generation on large dams, artisanal fisheries, and frequent flooding events that impact greatly on local populations, the plume has not been well studied. Observations during the period 2004–2007, when the winds were mainly easterly or south-easterly, indicated that the plume waters can extend both downstream (equatorwards) and upstream (polewards) of the Zambezi Delta with a recirculating bulge near the river mouth. The model is constructed using the Regional Ocean Modeling System (ROMS), with a 40-km long, 3-km wide river discharging into a rectangular coastal ocean with a linearly sloping bottom. When the model is forced only by a constant river discharge of $1\,000\text{ m}^3\text{ s}^{-1}$ (typical of observed discharge amounts in summer), the Kelvin and Froude numbers for the resulting plume imply a ‘large-scale’ buoyant discharge with a coastal current that is close to being in geostrophic balance with the across-shore pressure gradient and a recirculating ageostrophic bulge near the mouth. The distributions of the bulge and plume waters are found to be relatively insensitive to the discharge amount. Under constant wind forcing, the plume distribution changes dramatically. Northerly and easterly winds produce the largest changes with the latter able to deflect the plume up to 180° due to Ekman drift. When sea breeze-like winds are imposed, accumulation of water in the bulge occurs with substantial spreading upstream. Stronger sea breezes lead to less downstream spreading of the plume than gentle winds. When the winds are mainly across-shore, Ekman drift dominates, but the dynamics become almost geostrophic when the winds are roughly aligned to the coast. These experiments suggest that the Zambezi River plume is sensitive to the winds on diurnal to synoptic time-scales.

Keywords: dynamics, ROMS modelling, wind forcing

Introduction

Freshwater discharges from river mouths have important influences on many coastal regions including coastline alteration, the transport and dispersion of sediments and pollutants, and changes in the productivity and availability of biological resources (Mann and Lazier 2013). In this study, the little-studied Zambezi River plume is considered. The Zambezi River is the largest river on the eastern seaboard of Africa and empties through a wide delta onto the Sofala Bank on the western boundary of the Mozambique Channel around $18^\circ\text{--}19^\circ\text{ S}$, $36^\circ\text{--}36.5^\circ\text{ E}$. This channel is about 1 600 km long and ranges between 300 and 950 km wide, and is largely separated from the South Indian Ocean by the island of Madagascar. The Zambezi River’s high sediment flux has extended the delta seaward on geological time-scales (Walford et al. 2005). Flooding of the delta and upstream regions often occurs due to heavy summer rainfall and sometimes on account of poor management of the inland dams (Kariba in Zimbabwe and Cabora Bassa in Mozambique), which causes great hardship and devastation to the poor rural population that depends on subsistence agriculture (Usman and Reason 2004; Reason et al. 2005; Manhique et al. 2011). Artisanal fisheries (mainly shrimp) are also strongly impacted by variations in the Zambezi River discharge and subsequent plume behaviour (Mann and Lazier 2013).

The Zambezi River outflow has a mean discharge rate of $3\,000\text{ m}^3\text{ s}^{-1}$ (Gammelsrød 1992) but during the 2004–2007 summer sampling period reported on by Nehama (2012) and Nehama and Reason (2014), typical values were of order $1\,000\text{--}2\,000\text{ m}^3\text{ s}^{-1}$ in 2004 and 2006 with larger amounts in 2005 and 2007 (a maximum of almost $10\,000\text{ m}^3\text{ s}^{-1}$ was observed in the second week of February 2007). The discharge is believed to have an influence, not only on the nearshore hydrodynamics and ecosystems, but also on the offshore mesoscale circulation, particularly when the fresh water from runoff dominates the water masses on the continental shelf (Sætre and da Silva 1984; Schumann 1998). Lutjeharms (2006) presented evidence that the seaward intrusion of fresh water from the Zambezi River can reach up to 50 km offshore and was confined to the upper 15–30 m.

Despite various studies conducted along the Sofala Bank in recent years, as well as the proposed linkages between the Zambezi River discharge and secondary production (IMR 1977, 1978a, 1978b; Scodanibbio and Mafiez 2005), the outflow patterns from the river have not been reported to date other than in a PhD thesis (Nehama 2012) and in the brief descriptive synthesis of Nehama and Reason (2014). Here, the Zambezi River plume is studied in more

detail using an idealised numerical model. The purpose of the modelling was to assess the basic dynamics of the plume and its sensitivity to discharge intensity and to different wind forcing.

Material and methods

An idealised modelling study of the Zambezi River plume is presented which consists of a rectangular basin of width 210 km and length 660 km and which represents the central part of the western half of the Mozambique Channel. The model results were extensively validated in the PhD thesis of the first author (Nehama 2012) using observations made each summer from 2004 to 2007, when the Mozambican National Institute of Fisheries Research carried out an oceanographic cruise over the Sofala Bank region (Figure 1).

Model description

The simplest model that could be constructed to understand the basic dynamics of the Zambezi River plume consists of a mean buoyancy source emptying into a monotonically sloping coastal ocean (to represent the Sofala Bank and adjacent Mozambique Channel) with no tidal or wind forcing. This configuration was set up in the Regional Ocean Modeling System (ROMS) to begin with in order to determine whether the basic gravitational adjustment of this tropical coastal ocean to a buoyant river source has any similarity to any of the observations of the Zambezi River plume. Subsequent to the analysis of this initial experiment, and motivated by observations of the river discharge and the regional winds, further model experiments were then performed with varying winds and different values of discharge to assess the plume sensitivity to these factors.

The IRD version of ROMS, known as ROMS AGRIF (Debreu et al. 2012), was used. ROMS is a free-surface, terrain-following ocean model that solves the three-dimensional hydrostatic primitive equations (Shchepetkin and McWilliams 2003, 2005) and has been widely applied in the Mozambique Channel and neighbouring western Indian Ocean (Hermes and Reason 2008, 2009a; Collins et al. 2014; Halo et al. 2014; Manyilizu et al. 2014).

In all model experiments, the connecting slope between the river mouth and the coastal ocean is assumed to be a constant 1/1 800, which is close to the real slope. A constant depth of 10 m is assumed for the river member, which is taken as 40 km long and 3 km wide (5 grid points). This length is about half the maximum distance of tidal influence upstream in the Zambezi River and is many times the value of the Rossby radius (about 4 km). Thus, this length is sufficient to allow the gravitational adjustment between the fresh and saline waters to occur before the river reaches the coastline, thereby ensuring that the fresh water enters the sea through an appropriate number of vertical grid points.

The coastal ocean has a western wall (the side where the Zambezi River is located) that is 10 m deep, and the depth increases monotonically from this wall to the eastern boundary (Mozambique Channel) where the depth is about 100 m. The ocean domain is 210 km wide (east–west) by 660 km long (north–south) with the estuary centre-line located 160 km from the southern boundary. This configuration was set up on an f -plane centred on the latitude of

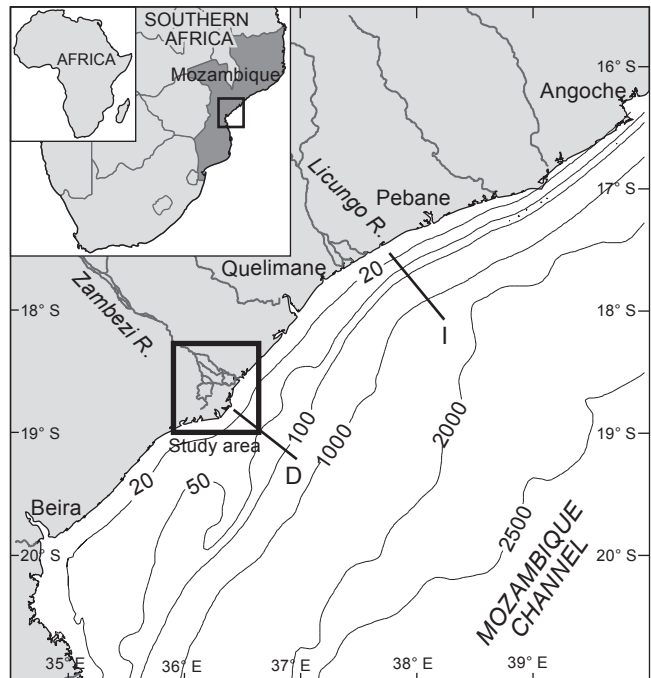


Figure 1: Map showing study region and location of across-shore transects D (offshore of the Zambezi Delta) and I (offshore of a point north of the Licungo River mouth). The 20, 50, 100, 1 000, 2 000 and 2 500 m depth contours are shown. The Sofala Bank is roughly demarcated by the coastline to the 100 m depth contour and extends from near 21° S in the south to about 17° S in the north

the Zambezi River mouth (18.83° S). Horizontal resolution ranged from 0.6 km at the mouth to 3.5 km at the eastern boundary with 20 σ -layers in the vertical. The latter are chosen such that the river member has a uniform vertical grid whereas the open ocean has resolution concentrated in the upper layers (about 1 m resolution in the upper 5 m). All four horizontal boundaries are set open so that fresh water can be introduced at the western boundary, and if tides are to be included, they can then propagate through the eastern boundary.

Initially, the model is at rest with no vertical displacement of the water surface. The model temperature is uniformly distributed throughout the domain and kept at 29 °C so that it is only salinity changes that cause the density to vary and that mark the plume extent in the domain. The initial salinity distribution ranges from 20.5 in the river member to 35.5 at the mouth and throughout the open ocean, as is typically observed (Sætre and da Silva 1984; Siddorn et al. 2001). This choice of a non-zero initial salinity in the upstream part of the river member (i.e. a non-fresh discharge) implies a shorter time for geostrophic adjustment and allows for the simulation of a realistic estuarine plume. It was found in experiments with a totally fresh ($S = 0$) initial salinity in the upstream part of the river that an unrealistically fresh plume (salinity of order 15) occurred immediately downstream of the mouth. The river discharge is ramped through a ‘tanh’ function over the first inertial period (1.55 days) to avoid high-frequency oscillations excited by an impulsive forcing. The maximum imposed discharge ranged from 1 000 to

8 000 m³ s⁻¹ in different experiments as is roughly observed during times of weak and high discharge (Sætre and da Silva 1984; Siddorn et al. 2001).

In experiments that impose idealised wind forcing, these winds are also ramped up through the first inertial period and then kept constant until the end of the simulation (100 days). A constant drag coefficient (C_d) of 0.0013 and air density of 1.2 kg m⁻³ are used to calculate the wind stresses. Bottom stress in the model follows a logarithmic formulation with the bottom roughness assumed to be $z_o = 0.01$ m. Passive lateral boundaries use Orlanski radiation conditions whereas active boundaries use Flather conditions for the normal and Chapman conditions for the tangential component of the barotropic velocity, respectively. The boundary conditions for the baroclinic velocity and tracers are set to Orlanski everywhere except at the western boundary where upwind conditions are used for tracers. The boundary conditions result in a barotropic flow that was uniform in the alongshore direction in experiments with the discharge and the winds turned off and, when the discharge is non-zero, in alongshore density-driven currents that could flow smoothly across the downstream boundary.

Lateral mixing of momentum and tracers occurs through Smagorinsky diffusion whereas vertical mixing uses the K -profile parameterisation (Large et al. 1994) amended for shallow-water flows by Durski et al. (2004). The plume behaviour is analysed in terms of the non-dimensional salinity anomaly s , defined by Garvine (1999) as:

$$s = (S_a - S) / (S_a - S_m)$$

where S_a is the reference (shelf) salinity initially set uniform at 35.5, S is the salinity computed by the model at each grid point and S_m is the surface salinity at the river mouth. Then, the isopleth $s = 0.1$ is taken as the effective boundary of the plume.

Results

The observations made during the summers of 2004–2007 (Nehama 2012; Nehama and Reason 2014) showed that the Zambezi River plume behaviour and distributions of surface salinity varied substantially over the Sofala Bank. This period was also characterised by considerable variations in measured river discharge upstream at Tete (440 km upriver from the delta) and in wind estimates near the delta (Nehama 2012; Nehama and Reason 2014). Due to a lack of any meteorological station data nearby, the regional winds were estimated from QuikSCAT satellite data and averaged over a 2° × 2° box centred offshore from the delta. In an attempt to understand better the plume and its sensitivity to discharge intensity and regional winds, the analysis of an idealised model of the plume is presented below.

Numerical model

Model plume with no wind forcing

Figure 2 shows snapshots of salinity anomaly, streamlines and currents at the surface for various times after the model is initialised with a river discharge of 1 000 m³ s⁻¹. The observed river discharge was of order 1 000–2 000 m³ s⁻¹ for most of the sampling period in 2004 and 2006 but was substantially

stronger in 2005 and, especially, in 2007, when it reached nearly 10 000 m³ s⁻¹ during the second week of February (Nehama 2012; Nehama and Reason 2014). This section first describes the model response to a discharge of 1 000 m³ s⁻¹ and then its response to larger discharge amounts.

It is evident that the model response to the discharge of 1 000 m³ s⁻¹ is a growing anticyclonic bulge and a developing coastal current which is already apparent within 10 days. Numerical simulations of buoyant plumes often produce a relatively weak alongshore current and a recirculating bulge that continually grows (Garvine 1999; Fong and Geyer 2002; Cheng and Casulli 2004; Hetland and Signell 2005; Isobe 2005), because it is impossible to balance the alongshore momentum flux in this case on either an f -plane (as used here) or a β -plane (Pichevin and Nof 1997; Nof and Pichevin 2001). This imbalance also leads to upstream flow of the plume in the opposite direction to Kelvin wave propagation but of weaker magnitude than the downstream counterpart (Pichevin and Nof 1997). Laboratory experiments of unforced river plumes also show this behaviour (Avicola and Huq 2003; Horner-Devine et al. 2006). Many real-world river plumes also show bulges (e.g. Chant et al. 2008; Horner-Devine 2009; Hickey et al. 2010; Warrick and Stevens 2011). However, bulge growth itself has not been clearly observed, presumably due to local wind effects disrupting this growth. The observations (Nehama 2012; Nehama and Reason 2014) suggest that the Zambezi River plume had characteristics of a bulge in 2004, 2005 and 2007.

The spread of the leading edge of the plume ($s = 0.1$) can be seen in Figure 3 along with that of the coastal current and the bulge. Whereas the leading edge spreads rapidly in the first 15–20 days, there is a sharp deceleration over the next ~20 days as geostrophic adjustment starts to dominate. As a result of this adjustment, the spread of fresher plume waters ($s > 0.1$) reaches its maximum northward (downstream) position at about day 70, after which the waters retreat slightly back towards the river mouth. The width of the coastal current slowly increases towards a maximum around day 70, after which it is roughly constant, whereas the bulge continues to grow throughout the simulation. The maximum depth of the bulge is about 5 m after 50 days of simulation (not shown).

Various non-dimensional numbers can be estimated to give an indication of the dominant dynamics. The Rossby number R_o , based on the velocity of the freshwater flow exiting the mouth U_o and the width of the mouth L (3.11 km), is defined as $R_o = U_o / fL$, where f is the Coriolis parameter. At day 50, which Figure 3 shows to be when the plume is well established in the domain, $U_o = 0.04$ m s⁻¹ giving $R_o = 0.27$, a relatively small value that implies that the shape of the bulge should be semi-circular with its centre relatively close to shore (Fong and Geyer 2002), which is consistent with Figure 2. The Kelvin number $K = L / L_r$, where L_r is the baroclinic Rossby radius, determines the length scale over which inertial forces remain important compared to the Earth's rotation (Geyer et al. 2000; Warrick et al. 2004). L_r is defined by C / f , where C is the phase speed of the first baroclinic mode. For the plume simulated here, $C = 0.18$ m s⁻¹ at the mouth and $L_r = 3.81$ km, so with the river width at the mouth being 3.11 km, $K = 0.82$. Because this value

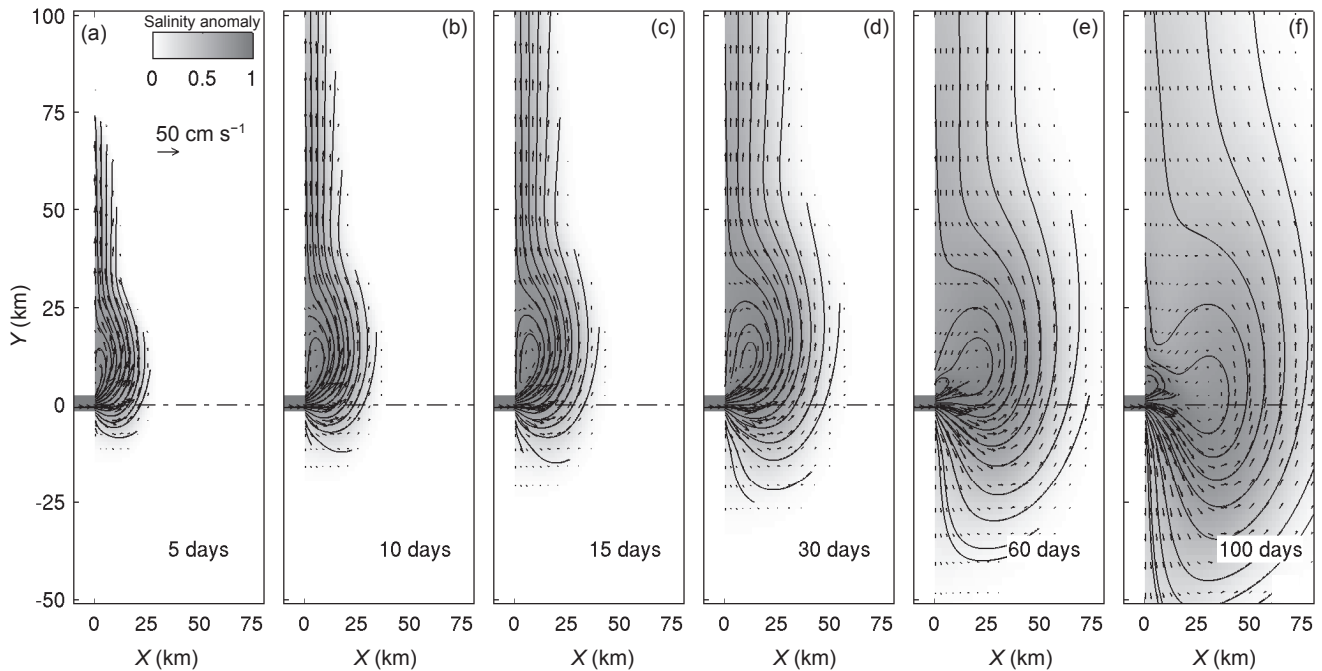


Figure 2: Snapshots of the bulge migration beginning 5 days after the initialisation of the discharge through to the end of the simulation (100 days). Salinity anomalies are contoured in grey scale and streamlines leaving the river mouth are shown. The axes represent distance from the river mouth and the panels (a)–(f) denote various times after model initialisation

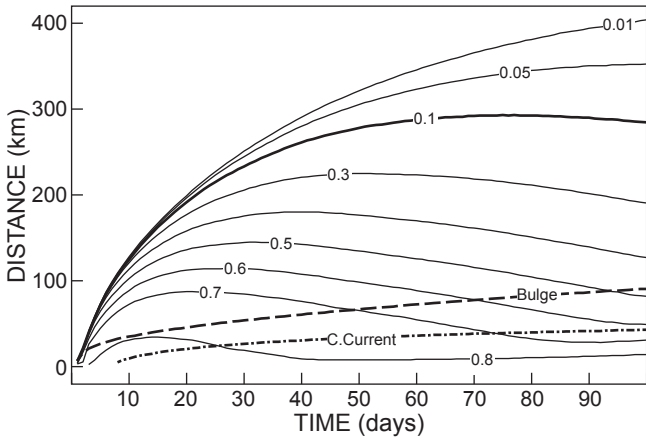


Figure 3: Evolution with time of the coastal current in the alongshore direction (thin lines) with the plume boundary (the 0.1 isopleth) in bold, its width at a point 100 km downstream from the mouth (dash-dot line) and the seaward advance of the bulge (dashed line). ‘C.Current’ refers to the coastal current

is close to but less than unity, the buoyant flow is expected to cover the entire width of the river outflow (Huq 2009) and both inertial and Coriolis forces are important. However, farther downstream, the characteristic length scale L should be taken as the across-shore extent of the plume. Typical values here are $L = 33.5$ km and $L_r = 2.50$ km, since $C = 0.12$ m s⁻¹. These values give $K = 13.4$ for the plume as a whole and thus indicate the importance of the Earth’s rotation (Garvine 1995; Kourafalou et al. 1996a). It is useful to consider the Kelvin number along with the Froude number ($F = U_o / C = 0.22$) (Kourafalou et al. 1996b). In this case,

K is large and F is small, typical of a ‘large-scale’ buoyant discharge (Garvine 1995), which is characterised by relatively slow flow (weak advection) and the importance of the Earth’s rotation throughout. As a result, the alongshore extent of the coastal current becomes large compared to the bulge width. The flow will not be in geostrophic balance as it leaves the river mouth and the Coriolis force causes it to turn to the left in the Southern Hemisphere. However, as it turns to the left, the blocking coastline exerts an opposing pressure gradient in the form of a slope in sea level. Part of the buoyant plume water continues downstream as a coastal current that is relatively close to being in geostrophic balance, and the other part recirculates as a bulge in front of the river mouth (Fong and Geyer 2002).

In many cases, this bulge circulation can be assumed to be in gradient wind or cyclostrophic balance (Yanovsky and Chapman 1997; Isobe 2005; Horner-Devine et al. 2006). Figure 4 plots the terms in the momentum balance along an across-shore transect through the bulge with Figure 4d showing the gradient wind terms. It is seen that the centrifugal term is smaller than the Coriolis and pressure gradient terms that more or less mimic each other throughout the simulation. The error in gradient wind balance is plotted in Figure 4e and the remaining error terms in Figure 4f. From these, it is apparent that the error in gradient wind balance is quite large with its maximum occurring at the edge of the core region. The other error terms are an order of magnitude smaller than the gradient wind terms which means that none can fully account for the discrepancy in the gradient wind balance. All the diffusive terms are considerably smaller than those in Figure 4f and hence are not shown. The small but non-zero radial acceleration is consistent with the bulge expanding but the leading edge of

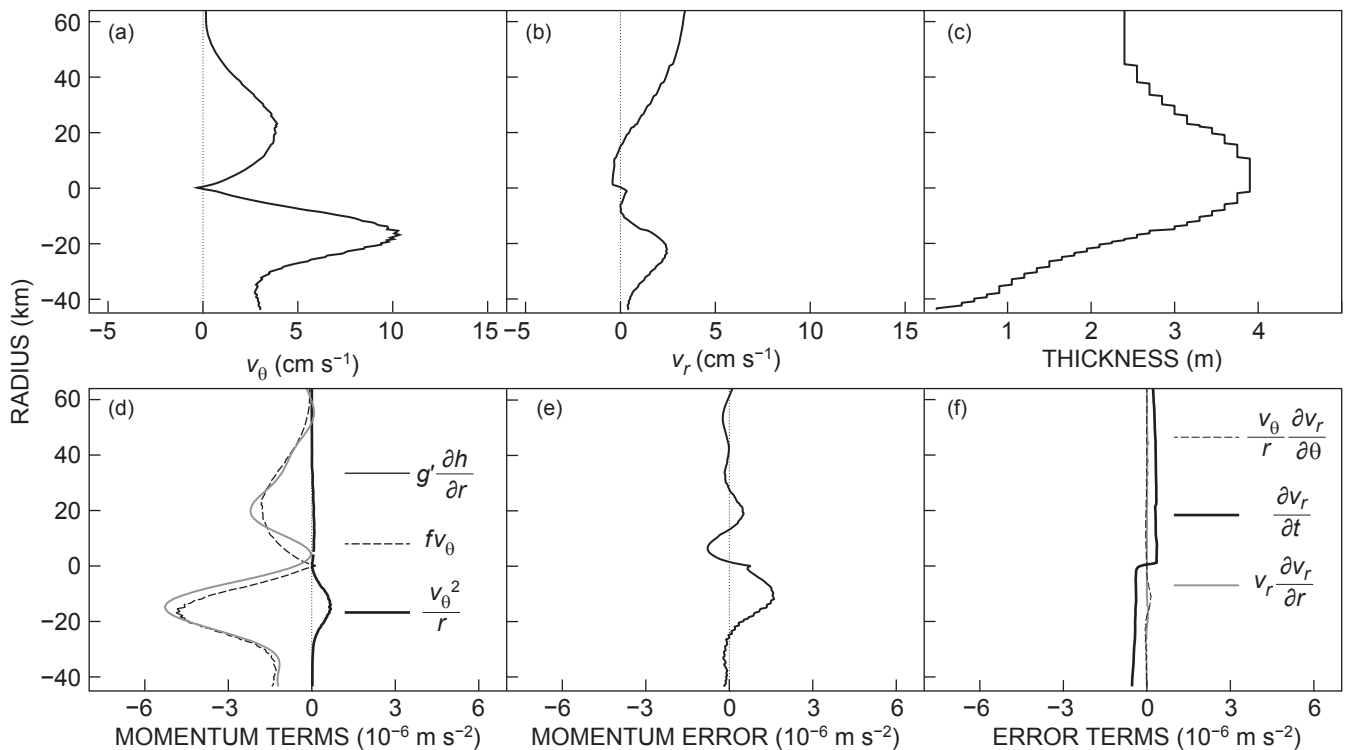


Figure 4: Momentum balance of the bulge evaluated after 50 days of model integration. The velocities in (a) and (b) have been averaged through the plume. A filter has been applied to smooth out high-frequency oscillations in the various terms in the momentum equation expressed in cylindrical polar coordinates (e.g. Isobe 2005)

the plume reaching a near-steady state (at about 70 days; Figure 3). Thus, growth of the bulge is an important part of the momentum balance of the bulge, but it is insufficient to complete the balance.

A transect across the plume at a point 200 km downstream from the river mouth on day 50 of the simulation indicates that the plume occupies the uppermost few metres with a downstream flow of about 0.05 m s⁻¹ (not shown). Offshore and beneath this buoyancy-driven circulation is an ambient flow in the opposite direction, which reaches a maximum of not much more than 0.005 m s⁻¹ near a point about 25 km offshore from the mouth and at about 15–20 m depth (not shown). Thus, a vertical current shear exists between this flow and the plume. Integrating across the plume at this point ($y = 200$ km) results in a freshwater transport of 191.2 m³ s⁻¹, or about 19% of the initial discharge from the river mouth, which is evident at this downstream transect of the plume.

Figure 5 shows the terms in the vertically integrated momentum balance with Figure 5b indicating that the bottom pressure term is stronger than Coriolis. In the x -direction (Figure 5a), the geostrophic terms are two or more orders of magnitude larger than local acceleration, advection, bottom stress and diffusion. The Coriolis term in Figure 5d indicates that the across-shore velocity is very small and positive. Figure 5c shows that the geostrophic terms are also the largest in the momentum balance in the y -direction, but now the diffusive terms are sizeable. Also non-negligible is the local acceleration that decreases from the coast to the offshore boundary.

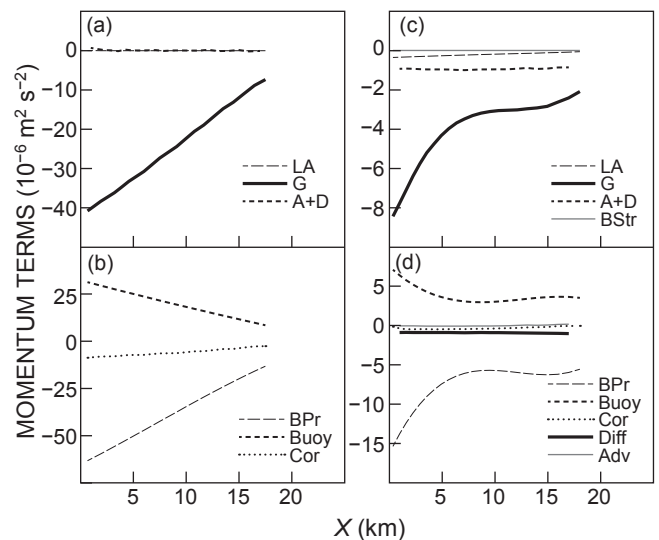


Figure 5: Vertically integrated terms in the momentum equation calculated at $t = 50$ days for an across-shore transect located 200 km downstream of the river mouth. Panels on the left (right) are for momentum in the across-shore (alongshore) direction. The top panels show all the terms in the balance while the bottom panels show only the dominant terms. Velocities and densities are averaged through the plume thickness. LA = local acceleration, G = geostrophic, A+D = advection (Adv) and diffusion (Diff), BStr = bottom stress, BPr = bottom pressure, Buoy = buoyancy, and Cor = Coriolis

Sensitivity of the plume to discharge strength and wind

The previous section shows that the idealised Zambezi River model plume under a typical discharge has basic characteristics that are consistent with previous observational, theoretical and numerical studies of river plumes elsewhere in the world, thereby providing confidence in the model. Thus, in this section, the sensitivity of the plume dynamics to different discharge amounts and to different wind forcing is studied. Model experiments were performed in which this discharge was varied from 1 000 to about 8 000 m³ s⁻¹ (as is typically observed – Nehama 2012; Nehama and Reason 2014), leading to the plumes shown in Figure 6 after 50 days of simulation. Note that a real-world maximum discharge of almost 10 000 m³ s⁻¹ was observed in 2007. The plume structures in Figure 6 are more or less the same in each case except that larger freshwater discharge produces slightly larger plumes and hence enhances the relative freshness of the inshore water. As the size of the bulge increases, the amount of fresh water upstream of the river mouth also increases, yet the brackish water in this region is part of the recirculating bulge and is always attached to the coast. However, in some of the observations of the Zambezi River plume (Nehama 2012; Nehama and Reason 2014), the brackish water to the south is separated from the coast. In any case, Figure 6 suggests that river discharge alone is unlikely to promote the upstream spreading of plume waters beyond about 50 km from the mouth.

An obvious factor that may lead to such upstream spreading is local wind forcing. To test this, model runs were performed as before but with constant wind forcing imposed in one of the four major directions. Two sets of experiments were conducted, one set with weak winds (5 km h⁻¹) and the other with moderate winds (12 km h⁻¹). Although the observations reported by Nehama (2012) and Nehama and Reason (2014) show times of variable winds, there are also quite lengthy periods when the winds are relatively steady so it is useful to use constant wind forcing to begin with.

Figure 7 shows the results of these experiments after 50 days of integration, long enough for the plume to adjust to the forcing. The results can be interpreted to reasonable accuracy using the analytical solutions of Chao (1988) for the linearised momentum equations in a shallow coastal sea and consist of a buoyant highly stratified plume spreading on top of an inert layer. In that framework, the resulting flow consists of a surface Ekman drift generated by the wind and a geostrophic current that varies with distance offshore from the coast.

When northerly (upwelling-favourable) weak winds are imposed on the channel (Figure 7e), there is a seaward movement of the plume and marked weakening of the nearshore stratification. Under moderate northerly winds (Figure 7a), a coastal current does not obviously occur because the Ekman drift opposes the density-driven circulation. In this case, there is a tongue of river water leaving the mouth that weakens offshore due to mixing with the ambient water. For the weak-wind case (Figure 7e), the wind mixing is reduced and the plume stratification offshore increases. Plume waters then spread offshore along the estuary axis and are also able to move about 50 km downstream (in the sense of a Kelvin wave).

Westerly (seaward-blowing) winds enhance the freshwater transport from the river onto the shelf, and enhance the stratification. The Ekman drift is now in the same direction as the density-driven current, leading to plume waters spreading strongly downstream. In the moderate-wind case (Figure 7b), offshore velocities are greater than inshore velocities, leading to a plume structure that seems to detach from the coast. For weak westerly winds (Figure 7f), the flow gradually decreases in the offshore half of the plume and the downstream extent of the plume exceeds the model domain.

Southerly (downwelling-favourable) winds lead to a wind-driven coastal current by driving the plume waters against the downstream coast. This current remains attached to the coast and is non-uniform as it contains both a parallel and a meandering flow. The meandering appears more pronounced for weak winds (Figure 7g). In both cases, the coastal current is narrowest and relatively stronger immediately downstream from the bulge region.

Easterly (landward-blowing) winds promote the withdrawal of fresh water from the shelf, weaken the nearshore stratification and therefore enhance the Ekman drift. This drift causes set-up of the sea surface against the upstream coast, which can drive a geostrophic flow if the wind forcing is weak (Figure 7h). The plume water is carried upstream by the Ekman transport and it forms either a pool of less-dense water in the moderate-wind case (Figure 7d) or a coastally-trapped flow in the weak-wind case (Figure 7h). In the latter case, some of the water also flows downstream in the sense of a Kelvin wave but at much slower speed. The action of the wind is to split the flow offshore of the mouth, with most of the water turning right to form the wind-driven coastal current and the rest proceeding downstream as the buoyancy-driven part. In both weak and moderate wind cases, the easterly wind is able to deflect the motion of a buoyant plume by up to 180°. This result is of considerable interest as the observed winds in the Mozambique Channel very often have a substantial easterly component.

The vertical structure of the flow is shown in Figure 8. The maximum plume thickness at about 10–15 km from the coast rarely exceeds 5 m except when the plume is forced by westerly winds. The broadest plumes were formed in the northerly wind case followed by the westerly wind case. In the easterly case, moderate winds lead to more mixing downwards of plume waters in the nearshore. In general, the plumes are slightly deeper and substantially broader when forced with weak winds than with moderate winds. An exception is for westerly wind forcing, which produces a deeper plume when the winds are stronger.

Given that the observed winds over the Sofala Bank during the season of maximum Zambezi River discharge (January–April) are mainly south-easterly, additional experiments were conducted with constant winds blowing from this direction. To investigate if there was any sensitivity to the southerly component being stronger than the easterly component, or vice versa, the wind directions were modified by up to 30° from the south-easterly direction. It was found that plume distributions were very similar to those for the southerly wind case with some small differences in length scales (not shown). The results imply that wind forcing that has a negative (onshore or easterly) component and a null or positive northward component leads to a sizeable

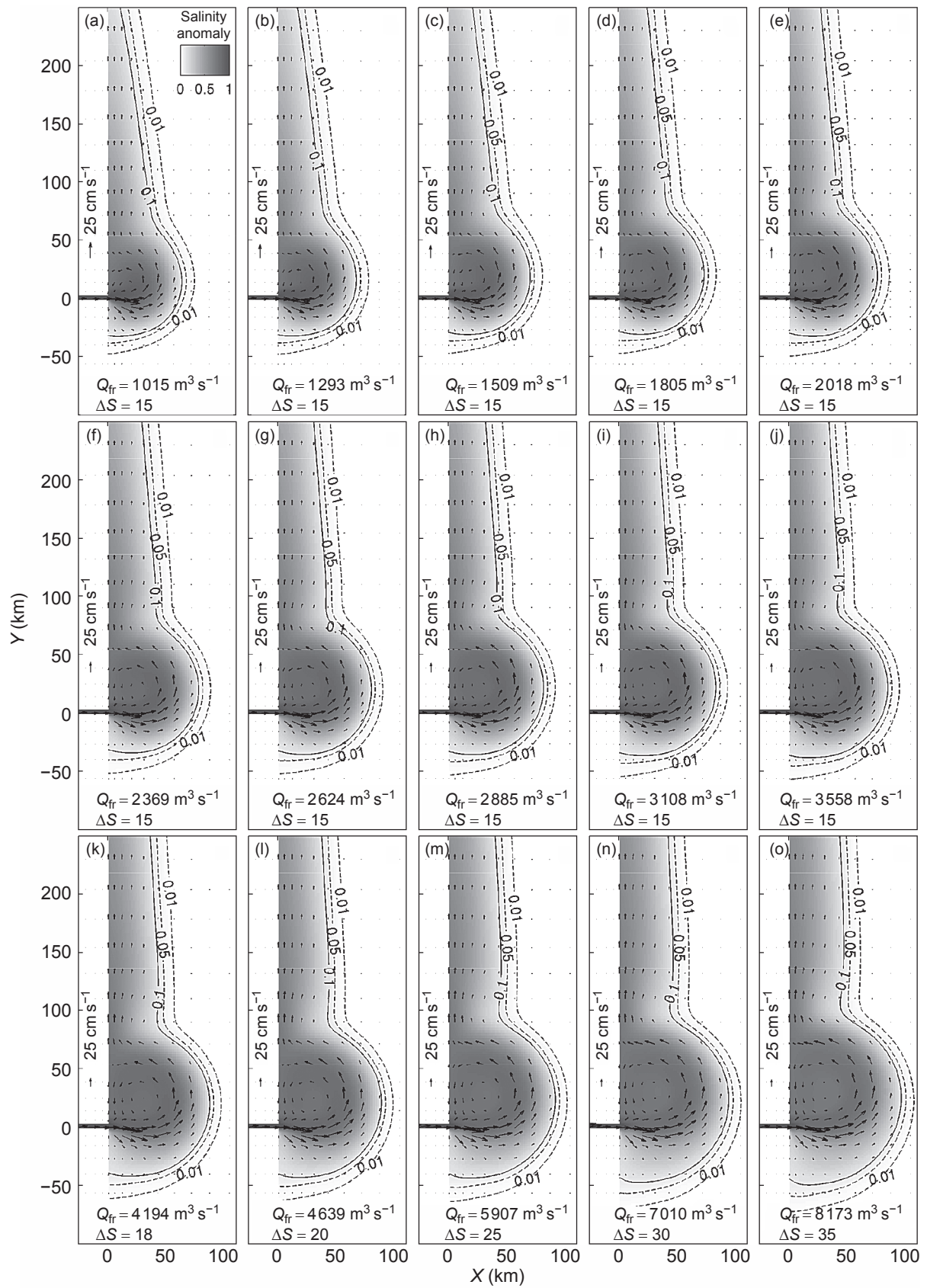


Figure 6: Surface salinity anomaly and velocity fields at time $t = 50$ days for different river discharge amounts Q_{fr} ranging from 1 015 to 8 173 $m^3 s^{-1}$. ΔS is the salinity difference between the plume and the ambient waters

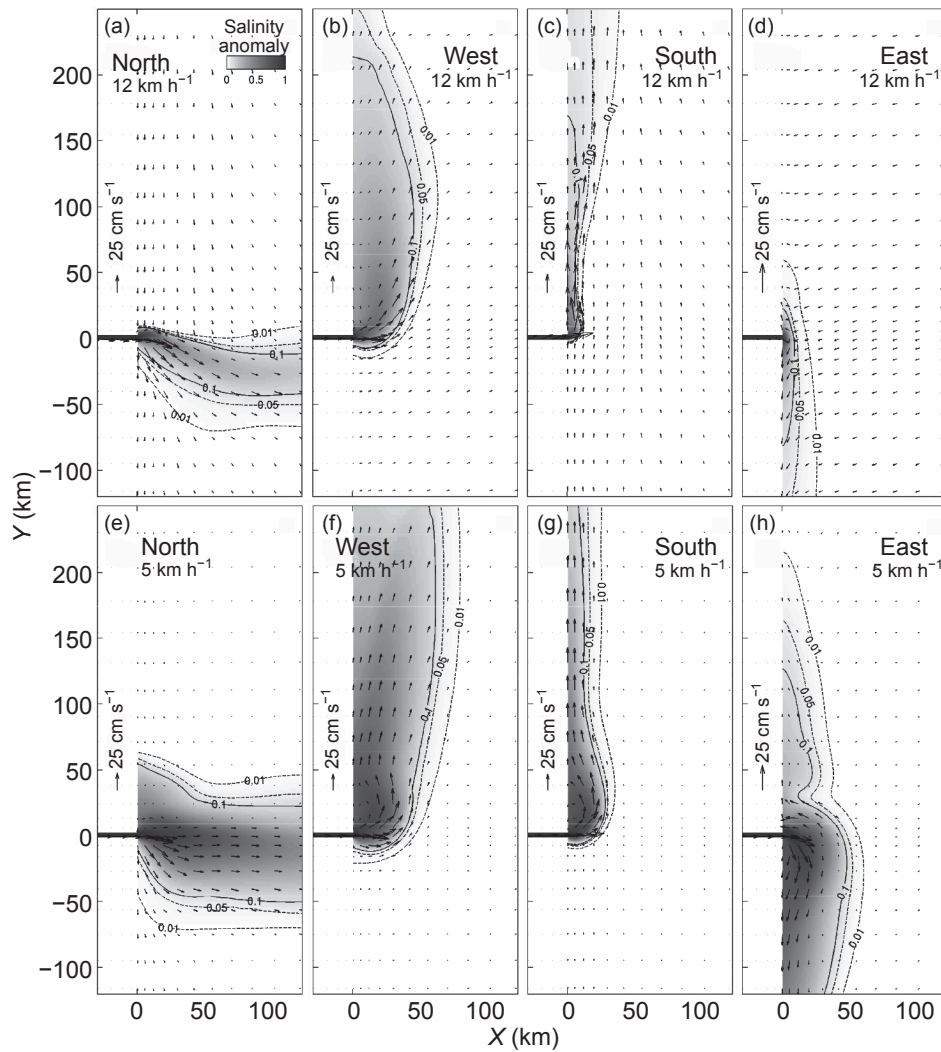


Figure 7: Surface salinity anomalies and velocities at time $t = 50$ days simulated under moderate (top) and weak (bottom) wind forcing. The wind blows from the direction stated in each panel. See text for further detail

upstream component of the plume, as is often observed (Nehama 2012; Nehama and Reason 2014). In all cases, the plume depth was very similar but the width increased as the winds become more easterly.

In the real world, the wind does not maintain a constant speed. To test the plume sensitivity to a change in wind speed, two more experiments were conducted. In the first case, a south-easterly wind at 5 km h^{-1} was imposed for the first 50 days after which the winds were ramped up to 12 km h^{-1} over half an inertial period (1.55 days). In the second experiment, the initial winds were south-easterly at 12 km h^{-1} and then decreased smoothly to 5 km h^{-1} after day 50, again over half an inertial period. Figure 9 shows the resulting plume behaviour after 7 days of changed wind speed forcing (i.e. at day 58).

In the strengthening case, the plume gradually adjusts by substituting the large pool of fresh water with a smaller bulge as is typical in the moderate wind-forcing case (cf. Figures 7g and 9a). The stronger winds erode the stratification offshore in the bulge region leading to a deeper

plume (Figure 9c). On the other hand, for the weakening wind case, the stratification near the river mouth increases followed by flow separation within the bulge (Figure 9b, d). In both scenarios, some signature of the initial plume is still noticeable, indicating that the plume takes a little longer than a week to fully adjust to the change in wind strength. Thus, the behaviour of the plume, while responsive to the wind blowing over the prior few days, also has sensitivity to wind strengths somewhat earlier than that. This result is of particular interest as the dominant spectral peaks in synoptic scale winds near the Zambezi Delta are at 12 days, and to a lesser extent, 6 days (Nehama 2012). Similar spectral peaks in coastal winds have been found elsewhere in tropical southern Africa (Risien et al. 2004; Hermes and Reason 2009b).

Response to oscillating winds

The final set of experiments used an idealisation of the observed sea-breeze cycle in the region with an ellipsoid of major axis oriented along the east-south-east direction

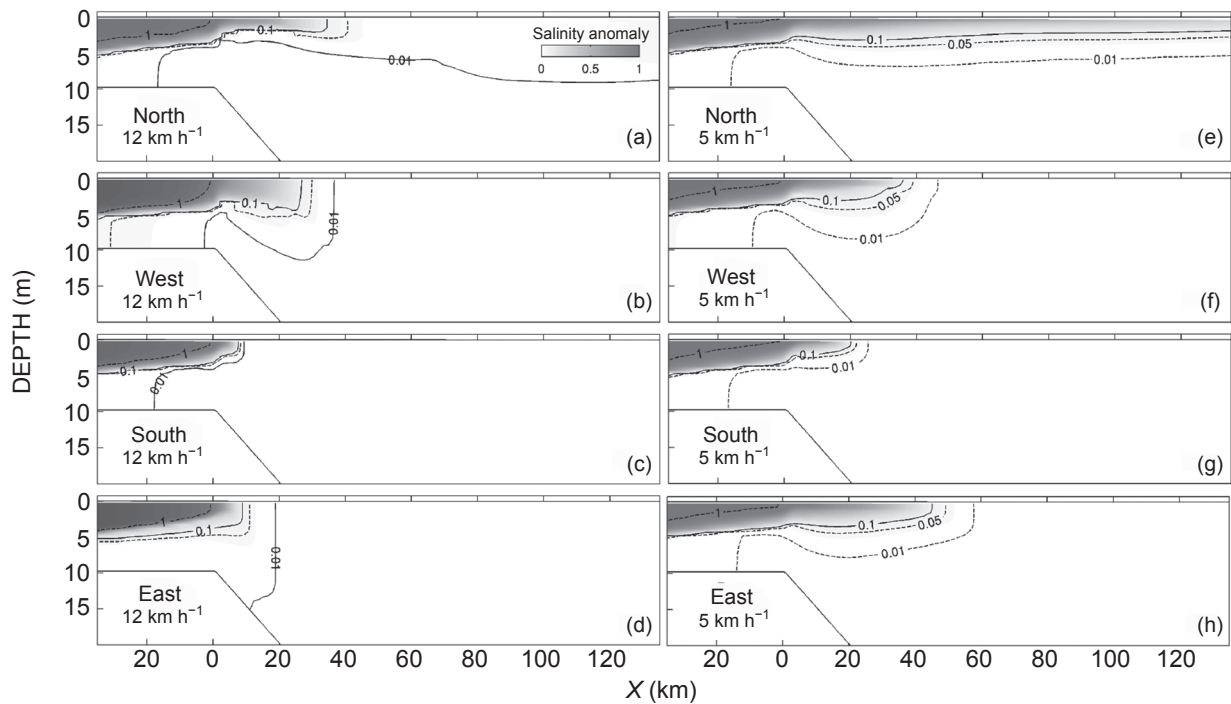


Figure 8: Vertical distribution of salinity at time $t = 50$ days along a transect through the river mouth perpendicular to the coast. The moderate (left panels) and weak (right panels) wind blows from the direction stated in each panel

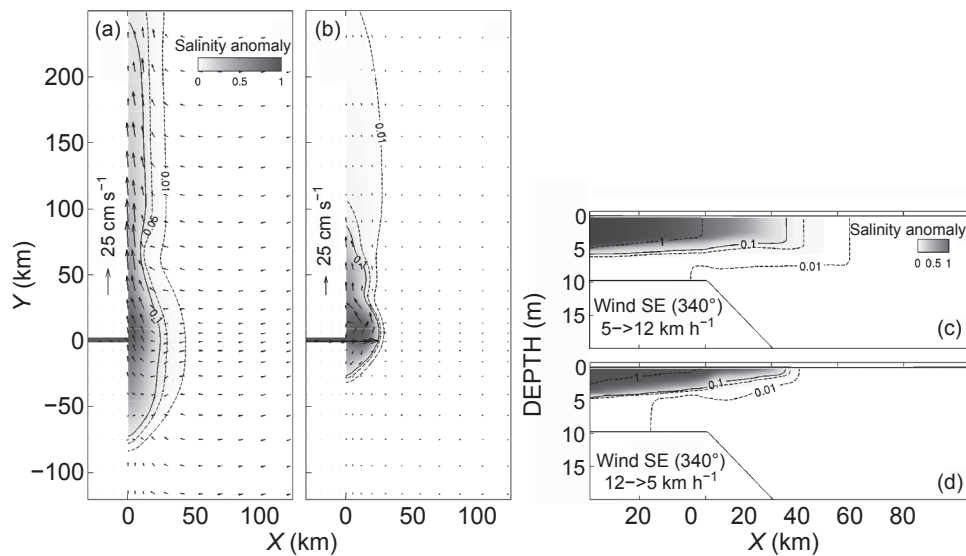


Figure 9: Horizontal and vertical structure of the plume 7 days after strengthening or weakening the south-easterly wind forcing between 5 and 12 km h⁻¹. The grey shading plots the variation in salinity anomalies at this time

of the sea breeze and varying diurnally. Different wind speeds of 5, 12, 18 and 26 km h⁻¹ were used in these experiments. Figure 10a shows the plume response after 50 days of forcing under constant, weak south-easterly winds and Figure 10b–e shows the response under sea breezes of different strengths that vary from landward to seaward over a 24-h period. The nearshore stratification increases considerably in response to the periodic wind field with enhanced mixing in the plume farther offshore.

Large changes in plume structure occur for sea breezes of maximum speed 12 km h⁻¹ and stronger (Figure 10c–e). The dynamics are dominated by Ekman drift at times when the wind is oriented mainly landward or seaward, and the flow becomes geostrophic when the winds are aligned with the coast. The plume water mainly spreads downstream under buoyancy with weak sea-breeze forcing (Figure 10b) and also accumulates in front of the bulge when the maximum winds are increased to 12 km h⁻¹ (Figure 10c).

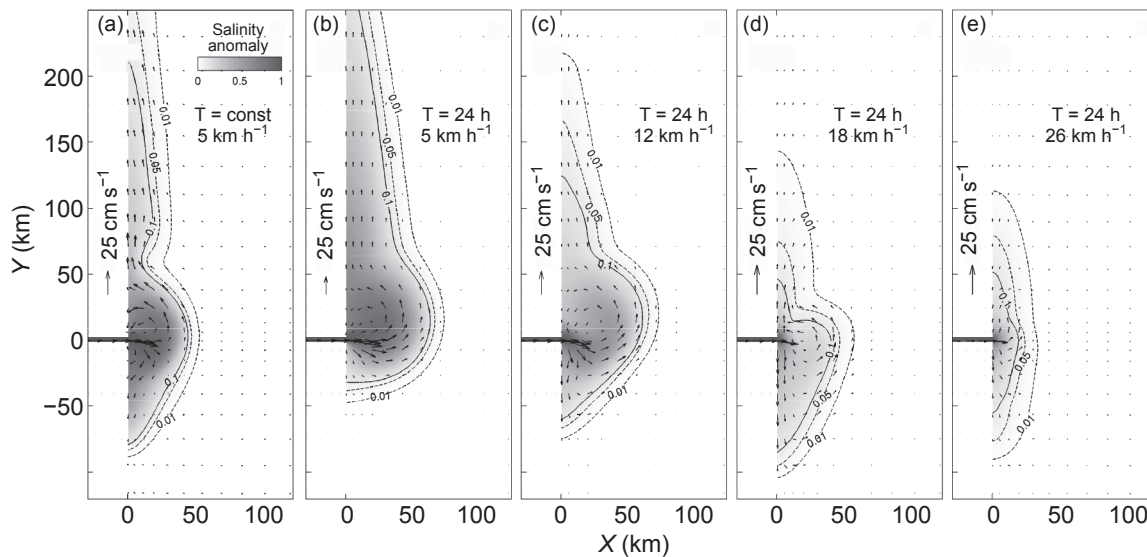


Figure 10: Surface salinity anomalies and velocities under different wind forcing (a) being of constant strength and south-easterly direction and (b–e) corresponding to sea-breeze forcing of different strength. Panel(s) labelled $T = \text{const}$ and $T = 24 \text{ h}$, respectively, refer to experiments where the wind forcing is held constant in time and where it varies as a sea–land breeze over 24 hours

For the stronger sea breezes (Figure 10c–e), there is also a significant upstream component to the plume. Furthermore, the stronger the sea breeze, the shorter the length of the downstream current.

Comparison of the vertical structure of the plume in these sea-breeze experiments (not shown) with the constant-wind case indicates that the sea breeze results in a less well-mixed water column near the plume front. Also, as the sea-breeze intensity increases, the stratification offshore is eroded, leading to a narrower bulge while, at the same time, the inshore mixing increases, deepening the plume and promoting the seaward movement of its base.

Discussion

As discussed in Nehama (2012) and Nehama and Reason (2014), shipboard observations made during periods of expected high Zambezi River discharge over four years (2004–2007) showed that the plume waters could spread substantially both equatorwards (or downstream, in the sense of Kelvin wave propagation) and polewards (upstream), as well as offshore of the mouth. At times, a bulge region near the delta was also apparent. Some periods of downstream spreading appeared consistent with theory for a buoyancy-driven flow in a two-layer coastal ocean (Garvine 1999) whereas other periods did not. To better understand the Zambezi plume during these periods of varying winds and discharge amount, the ROMS model was applied to the region. Initially the model was subjected to a constant discharge and subsequently it was forced with varying discharge amounts and then winds that varied in both magnitude and direction, including a sea-breeze-type circulation in the final set of experiments.

Analysis of the simplest model of the Zambezi River plume, in which a moderate freshwater source is released into a rectangular domain with a constantly sloping bottom, revealed some useful insights. Consistent with Nof and

Pichevin (2001) and Isobe (2005), the buoyant plume does not reach steady state due to the impossibility of achieving a geostrophic balance in this situation. Under a moderate discharge of $1\,000 \text{ m}^3 \text{ s}^{-1}$, the buoyant plume is confined to the upper 4 or 5 m with a downstream and offshore penetration of about 300 km and 75 km, respectively, after 100 days of integration. About half of this discharge contributes to the bulge area near the river mouth, about 30% is mixed with ambient water and the remaining 20% feeds the coastal current. The bulge is anticyclonic and continually grows slowly due to this momentum imbalance. However, regardless of the Zambezi River discharge amount, the upstream penetration is unlikely to extend beyond 50 km. Downstream, the buoyant coastal current is roughly in geostrophic balance with the across-shore pressure gradient.

Either relatively weak (5 km h^{-1}) or moderate (12 km h^{-1}) winds typical of the region can fundamentally alter the plume's behaviour when imposed as constant forcing. Easterly or south-easterly winds lead to substantial upstream flow, whereas northerly winds lead to a mainly offshore flow due to Ekman drift. Southerly winds induce a wind-driven coastal current that can meander and there is little bulge near the mouth. Observed winds almost always have a sizeable easterly component, with that from a direction somewhere between southerly and easterly being the most common. Thus, the model was also forced with a diurnally driven sea-breeze circulation whose major axis was south-easterly. Sea-breeze forcing at gentle to fresh intensity ($12\text{--}26 \text{ km h}^{-1}$) leads to marked changes in the plume characteristics compared to constant south-easterly wind forcing. There is an accumulation of plume water in the bulge region with noticeable upstream spreading. The downstream spreading of this water is noticeably less for the fresh sea breezes than for gentle sea breezes. For those times of day when the winds are directed mainly landward or seaward, Ekman drift dominates the dynamics but it becomes close to geostrophic when the wind direction is close to being aligned

to the coast. Furthermore, as the sea-breeze strength increases, the offshore stratification becomes more eroded, leading to a smaller bulge. At the same time, the nearshore mixing increases, deepening the plume and promoting the seaward penetration of the base of the plume.

Conclusion

An idealised ROMS model of the Zambezi River plume with wind forcing is able to capture many of the observed features of this plume. The response to varying discharge is non-linear, in that large increases do not lead to proportionally large changes in plume dimensions; an eight-fold increase in discharge roughly doubles the width of the bulge and the downstream plume width. Both wind direction and strength can fundamentally change the plume direction and strength if imposed for times that are long compared to an inertial period (about 1.5 days). Imposing diurnally varying winds (sea breezes) also produces pronounced changes in plume behaviour if these winds are at least 12 km h^{-1} in intensity. However, despite showing many realistic features, the model cannot account for presence of brackish water offshore and upstream that is detached from the coast and that is sometimes observed. To do so, the model may need to include more than one source of freshwater discharge as occurs in the real Zambezi Delta, as well as the effects of tides.

Acknowledgements — This study is based upon part of a PhD thesis by FPJN who gratefully acknowledges funding supplied by the Carnegie Regional Initiative for Sciences and Education network.

References

- Avicola G, Huq P. 2003. The characteristics of the recirculating bulge region in coastal buoyant outflows. *Journal of Marine Research* 61: 435–463.
- Chao S-Y. 1988. River-forced estuarine plumes. *Journal of Physical Oceanography* 18: 72–88.
- Chant RJ, Wilkin JL, Zhang W, Choi B-J, Hunter E, Castelao R et al. 2008. Dispersal of the Hudson River plume in the New York Bight: synthesis of observational and numerical studies during LaTTE. *Oceanography* 21: 148–161.
- Cheng RT, Casulli V. 2004. Modeling a three-dimensional river plume over continental shelf using a 3D unstructured grid model. In: Spaulding M (ed.), *Eighth International Conference on Estuarine and Coastal Modeling*, November 2003, Monterey, California. Reston, Virginia: American Society of Civil Engineers. pp 1027–1043.
- Collins C, Hermes JC, Reason CJC. 2014. Mesoscale activity in the Comoros Basin from satellite altimetry and a high-resolution ocean circulation model. *Journal of Geophysical Research* 119: 4745–4760.
- Debreu L, Marchesiello P, Penven P, Cambon G. 2012. Two-way nesting in split-explicit ocean models: algorithms, implementation and validation. *Ocean Modelling* 49–50: 1–21.
- Durski SM, Glenn SM, Haidvogel DB. 2004. Vertical mixing schemes in the coastal ocean: comparison of the level 2.5 Mellor-Yamada scheme with an enhanced version of the K profile parameterization. *Journal of Geophysical Research* 109: C01015.
- Fong DA, Geyer WR. 2002. The alongshore transport of freshwater in a surface-trapped river plume. *Journal of Physical Oceanography* 32: 957–972.
- Gammelsrød T. 1992. Variation in shrimp abundance on the Sofala Bank, Mozambique, and its relation to the Zambezi River runoff. *Estuarine, Coastal and Shelf Science* 35: 91–103.
- Garvine RW. 1995. A dynamical system for classifying buoyant coastal discharge. *Continental Shelf Research* 15: 1585–1596.
- Garvine RW. 1999. Penetration of buoyant coastal discharge onto the continental shelf: a numerical model experiment. *Journal of Physical Oceanography* 29: 1892–1909.
- Geyer WR, Hill P, Milligan T, Traykovski P. 2000. The structure of the Eel River plume during floods. *Continental Shelf Research* 20: 2067–2093.
- Halo I, Backeberg B, Penven P, Ansoorge I, Reason C, Ullgren JE. 2014. Eddy properties in the Mozambique Channel: a comparison between observations and two numerical ocean circulation models. *Deep-Sea Research II* 100: 38–53.
- Hermes JC, Reason CJC. 2008. Annual cycle of the South Indian Ocean (Seychelles-Chagos) thermocline ridge in a regional ocean model. *Journal of Geophysical Research* 113: C04035.
- Hermes JC, Reason CJC. 2009a. The sensitivity of the Seychelles-Chagos Thermocline Ridge to large scale wind anomalies. *Special Issue: Proceedings of the International Symposium on Effects of Climate Change on the World's Oceans. ICES Journal of Marine Science* 66: 1455–1466.
- Hermes JC, Reason CJC. 2009b. Variability in sea-surface temperature and winds in the tropical south-east Atlantic Ocean and regional rainfall relationships. *International Journal of Climatology* 29: 11–21.
- Hetland RD, Signell RP. 2005. Modeling coastal current transport in the Gulf of Maine. *Deep-Sea Research II* 52: 2430–2449.
- Hickey BM, Kudela RM, Nash J, Bruland KW, Peterson WT, MacCready P et al. 2010. River influences on shelf ecosystems: introduction and synthesis. *Journal of Geophysical Research* 115: C00B17.
- Horner-Devine AR. 2009. The bulge circulation in the Columbia River plume. *Continental Shelf Research* 29: 234–251.
- Horner-Devine AR, Fong DA, Monismith SG, Maxworthy T. 2006. Laboratory experiments simulating a coastal river inflow. *Journal of Fluid Mechanics* 555: 203–232.
- Huq P. 2009. The role of Kelvin number on bulge formation from estuarine buoyant outflows. *Estuaries and Coasts* 32: 709–719.
- IMR (Institute of Marine Research). 1977. Cruise report No. 1 of R/V *Dr. Fridtjof Nansen*. Joint NORAD/Mozambique/FAO project to investigate the fish resources of the coast of Mozambique. Institute of Marine Research, Bergen.
- IMR (Institute of Marine Research). 1978a. Cruise report No. 3 of R/V *Dr. Fridtjof Nansen*, January–March 1978. Joint NORAD/Mozambique/FAO project to investigate the fish resources of the coast of Mozambique. Institute of Marine Research, Bergen.
- IMR (Institute of Marine Research). 1978b. Cruise report No. 4 of R/V *Dr. Fridtjof Nansen*, April–June 1978. Joint NORAD/Mozambique/FAO project to investigate the fish resources of the coast of Mozambique. Institute of Marine Research, Bergen.
- Isobe A. 2005. The ballooning of river-plume bulge and its stabilization by tidal currents. *Journal of Physical Oceanography* 35: 2337–2351.
- Kourafalou VH, Lee TN, Oey L-Y, Wang JD. 1996a. The fate of river discharge on the continental shelf. 2: Transport of coastal low-salinity waters under realistic wind and tidal forcing. *Journal of Geophysical Research* 101: 3435–3455.
- Kourafalou VH, Lee TN, Oey L-Y, Wang JD. 1996b. The fate of river discharge on the continental shelf. 1: Modelling the river plume and the inner shelf coastal current. *Journal of Geophysical Research* 101: 3415–3434.
- Large WG, McWilliams JC, Doney SC. 1994. Oceanic vertical mixing: a review and a model with a nonlocal boundary layer parameterization. *Reviews of Geophysics* 32: 363–403.
- Lutjeharms J. 2006. The coastal oceans of south-eastern Africa.

- In: Robinson AR, Brink KH (eds), *The sea*, vol. 14B. Cambridge, Massachusetts: Harvard University Press. pp 783–834.
- Mann KH, Lazier JRN. 2013. *Dynamics of marine ecosystems – biological-physical interactions in the oceans*. Boston: Blackwell Scientific Publications.
- Manhique A, Reason CJC, Rydberg I, Fauchereau N. 2011. ENSO and Indian Ocean sea surface temperatures and their relationships with tropical temperate troughs over Mozambique and the Southwest Indian Ocean. *International Journal of Climatology* 31: 1–13.
- Manyilizu M, Dufois F, Penven P, Reason CJC. 2014. Interannual variability of sea surface temperature and circulation in the tropical western Indian Ocean. *African Journal of Marine Science* 36: 233–252.
- Nehama FPJ. 2012. Modelling the Zambezi River Plume using the Regional Ocean Modeling System. PhD thesis, University of Cape Town, South Africa.
- Nehama FPJ, Reason CJC. 2014. Morphology of the Zambezi River plume in the Sofala Bank, Mozambique. *Western Indian Ocean Journal of Marine Science* 13: 1–10.
- Nof D, Pichevin T. 2001. The ballooning of outflows. *Journal of Physical Oceanography* 31: 3045–3058.
- Pichevin T, Nof D. 1997. The momentum paradox. *Tellus* 49A: 298–319.
- Reason CJC, Hachigonta S, Phaladi RF. 2005. Interannual variability in rainy season characteristics over the Limpopo region of southern Africa. *International Journal of Climatology* 25: 1835–1853.
- Risien C, Reason CJC, Shillington F, Chelton DB. 2004. Variability in satellite winds over the Benguela upwelling system during 1999–2000. *Journal of Geophysical Research* 109: C03010.
- Sætre R, da Silva AJ. 1984. The circulation of the Mozambique Channel. *Deep-Sea Research* 31: 485–508.
- Schumann EH. 1998. The coastal ocean off southeast Africa, including Madagascar. In: Robinson AR, Brink KH (eds), *The sea*, vol. 11. New York: John Wiley & Sons. pp 557–581.
- Scodanibbio L, Mañez G. 2005. The World Commission on Dams: a fundamental step towards integrated water resources management and poverty reduction? A pilot case in the lower Zambezi, Mozambique. *Physics and Chemistry of the Earth* 30: 976–983.
- Shchepetkin A, McWilliams JC. 2003. A method for computing horizontal pressure-gradient force in an ocean model with a non-aligned vertical coordinate. *Journal of Geophysical Research* 108: 3090.
- Shchepetkin A, McWilliams JC. 2005. The Regional Oceanic Modeling system (ROMS): a split-explicit, free-surface, topography following coordinate oceanic model. *Ocean Modelling* 9: 347–404.
- Siddorn JR, Bowers DG, Hogue AM. 2001. Detecting the Zambezi River plume using observed optical properties. *Marine Pollution Bulletin* 42: 942–950.
- Usman MT, Reason CJC. 2004. Dry spell frequencies and their variability over southern Africa. *Climate Research* 26: 199–211.
- Walford H, White N, Sydow J. 2005. Solid sediment load history of the Zambezi Delta. *Earth and Planetary Science Letters* 238: 4–63.
- Warrick JA, Mertes LAK, Washburn L, Siegel D. 2004. Dispersal forcing of southern California river plumes, based on field and remote sensing observations. *GeoMarine Letters* 24: 46–52.
- Warrick JA, Stevens AW. 2011. A buoyant plume adjacent to a headland – observations of the Elwha River plume. *Continental Shelf Research* 31: 85–97.
- Yankovsky AE, Chapman DC. 1997. A simple theory for the fate of buoyant coastal discharges. *Journal of Physical Oceanography* 27: 1386–1401.